Materials and Design 193 (2020) 108837

Contents lists available at ScienceDirect

Materials and Design

journal homepage: www.elsevier.com/locate/matdes

Warm-forming of pre-aged Al-Zn-Mg-Cu alloy sheet

Johannes A. Österreicher [a,*], Matheus A. Tunes [b], Florian Grabner [a], Aurel Arnoldt [a], Thomas Kremmer [b], Stefan Pogatscher [b], Carina M. Schlögl [a]

[a] LKR Light Metals Technologies, Austrian Institute of Technology, Lamprechtshausenerstraße 61, 5282 Ranshofen, Austria
[b] Chair of Nonferrous Metallurgy, Department of Metallurgy, Montanuniversitaet Leoben, Franz-Josef-Straße 18, 8700 Leoben, Austria

HIGHLIGHTS

- Deep-drawing of pre-aged AA7075 sheet at 180 °C improves maximum draw depth and paint-bake response of designed parts.
- The process does not require solution heat treatment directly before forming.
- Optimization of energy use and production logistics is achieved.
- A potentially new hexagonal Mg/Zn nanoprecipitate is observed.

GRAPHICAL ABSTRACT

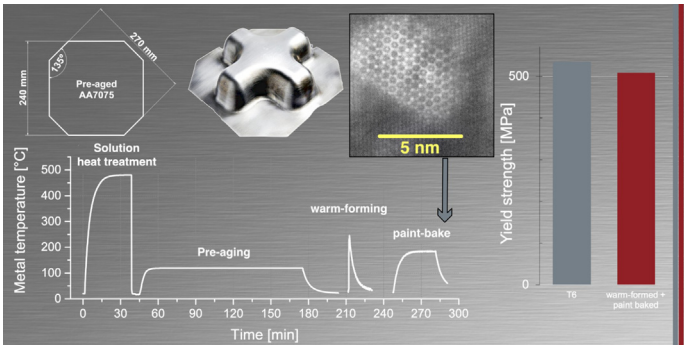

ARTICLE INFO

Article history:
Received 12 May 2020
Received in revised form 26 May 2020
Accepted 29 May 2020
Available online 6 June 2020

Keywords:
Aluminium
Automotive
Retrogression
Paint-bake
Deep-drawing
Transmission electron microscopy

ABSTRACT

Aluminium alloys of the 7xxx series are attracting the attention of automakers due to their high specific strength. However, widespread use of 7xxx series alloys for the production of car parts from sheet metal has so far been prevented due to their low formability at room temperature and the fact that conventional automotive paint-bake cycles are not suitable for aging the material to peak strength. Here we present an economic process chain for the deep-drawing of automotive parts from pre-aged AA7075 sheet at 180–250 °C that combines good formability with improved paint-bake response. The produced parts achieve roughly 95% of the peak-aged strength of AA7075. Precipitation during the production process is studied by differential scanning calorimetry and transmission electron microscopy.

© 2020 The Authors. Published by Elsevier Ltd. This is an open access article under the CC BY license (http://creativecommons.org/licenses/by/4.0/).

1. Introduction

Al-Mg-Zn(—Cu) alloys (7xxx series) are promising candidates for further lightweighting of cars [1–3]. However, their formability at room temperature is limited, thus making it difficult to form parts by deep-drawing [4,5]. For the same reason, crack-free self-pierce riveting is challenging [6–10].

Further complications arise from the process conditions in automotive industry: The age hardening of aluminium alloys is usually carried out simultaneously with curing of the paint at temperatures of approximately 143–205 °C for several minutes up to roughly 1 h in total [11]. In contrast, a widely-used peak age hardening regime of AA7075 is 120 °C for 24 h. Consequently, the peak aged state (T6) cannot be reached by paint-baking alone [6,12–15].

It was recently reported that pre-aging AA7075 at 120 °C can improve the material's paint-bake response so that near-T6 levels of strength can be reached [6,15,16]. Since the pre-aging temperature of

* Corresponding author.
E-mail address: johannes.oesterreicher@ait.ac.at (J.A. Österreicher).

https://doi.org/10.1016/j.matdes.2020.108837
0264-1275/© 2020 The Authors. Published by Elsevier Ltd. This is an open access article under the CC BY license (http://creativecommons.org/licenses/by/4.0/).

120 °C is the same as commonly used for T6 heat treatment, such pre-aged tempers are often referred as T6I4, standing for T6 treatment interrupted by natural aging. To elucidate the underlying mechanism of the improved paint-bake response, Lee et al. [16] performed transmission electron microscopy (TEM) of AA7075 pre-aged at 120 °C for 30 or 240 min. They found that during pre-aging, Guinier–Preston zones (GP-zones) are formed which do not completely dissolve during subsequent bake-hardening but rather act as nuclei for the η′ phase.

As mentioned above, the formability of 7xxx series alloys at room temperature is limited. Deep-drawing after solution heat treatment is practically impossible after only one day of natural aging, even for parts of low complexity [7,17,18]. To overcome this problem, W-temper forming and hot stamping/die quenching (referred to as hot stamping in the following) have been proposed [19,20]. However, the economic viability of both processes is limited by the need of solution heat treatment shortly before the deformation step [21] and quenching equipment (for W-temper forming) or cooled dies (for hot stamping). Even if these conditions are met, the paint-bake response of the parts with or without some time of natural aging is suboptimal [6,7,16,19,22]. Although pre-aging after W-temper forming or hot stamping could be beneficial, this would add yet another step to an already complex process chain.

An alternative to W-temper forming and hot stamping is warm-forming at temperatures of roughly 180–250 °C. This approach has been followed in several studies [5,12,23–27]. However, these reports focus mostly on warm-forming of the T6 temper. Where paint-baking was used, the T6-associated properties could not be restored after warm-forming.

The use of under-aged blanks to avoid over-aging was previously attempted at LKR/Austrian Institute of Technology as reported by Kumar and Ross [4] for a particular 7xxx series alloy with high Zn and low Cu content. While the maximum draw depth was greater than for T6 blanks, the yield strength after one-step or five-step paint-bake was inferior compared to paint-baked samples produced from T6 or T4 blanks, calling into question the economic viability of an additional pre-aging step. Long et al. [3] used experimental 7xxx series alloys in an under-aged temper for warm-forming. They reported higher strength than commercially available AA7055-T76 (which they used as a baseline). However, only limited experimental details and selected results were given.

In this work, we used pre-aged AA7075 blanks for deep-drawing at 180, 210, 230, and 250 °C. The parts were then subjected to a simulated paint-bake treatment at 185 °C. The maximum draw depth as well as the final mechanical properties were significantly improved compared to parts deep-drawn from blanks in T6 temper. Transmission electron microscopy as well as differential scanning calorimetry were used to study the precipitation of hardening phases.

2. Experimental

2.1. Material

AA7075-T6 sheet material of 2 mm thickness was used. Optical emission spectroscopy using a Spectro Spectromaxx 6 device gave the chemical composition presented in Table 1.

Similar material was used in previous studies [6,7]. Square-shaped blanks with cut corners (Fig. 1a) were produced so that two long sides of the blanks were parallel to the rolling direction of the sheet.

Table 1
Chemical composition of used AA7075-T6 sheet in wt%.

Zn	Mg	Cu	Si	Cr	Fe	Mn	Ti	Zr	Al
6.06	2.64	1.50	0.19	0.18	0.11	0.04	0.04	0.02	Balance

2.2. Heat treatments and deep-drawing

For solution heat treatment, a fraction of the produced blanks was placed in a pre-heated oven and kept at 480 ± 3 °C for 15 min (metal temperature as-measured using an embedded thermocouple, not including heating time of approximately 20 min) [28]. The blanks were quenched in water. Subsequently, the pre-aging heat treatment at 120 ± 3 °C for 2 h was performed in the same way but the blanks were allowed to cool in air to room temperature (RT) [6].

The blanks were then cleaned with isopropyl alcohol and lubricated using Moralub FB 100 Z produced by Molyduval. A cross-die deep-drawing tool (Fig. 1c) installed in a 160 t hydraulic double-sided press (see Fig. 1b and [4] for photographs) was used. The temperatures of the blank holder, die, and punch were controlled using a Plastic Service GmbH (PSG) profiTEMP hot runner controller connected to four thermocouples, mounted in the tool parts, eight electric resistance heating cartridges in the punch, and two heating coils each in die and blank-holder. The blank was inserted into the tool and the blank holder was closed with a pressure of 10 bar (20kN) so that the blank was heated by contact. After 30 s, deep-drawing at a speed of 5 mm/s was performed. The draw depth was raised or lowered in steps of 1 mm to determine the maximum draw depth were no through-thickness crack occured. For some blanks, the temperature evolution in the blank was measured by thermocouples embedded either in the fringe area or the center of the blanks. When the thermocouple was embedded in the center, a slit of approximately 2 mm was cut from the side of the blank to the center to accomodate the cable.

After deep-drawing, the parts were subjected to a simulated paint-bake treatment at 185 ± 5 °C for 20 min (plus heating time of 14 min) and allowed to cool to RT.

A profile of the complete process is given in Fig. 2. While the temperature curves are based on real process data, the delays between pre-aging and warm-forming and between warm-forming and paint-bake are not to scale, indicated by the broken line. These process steps were carried out within a few days. They are not considered time-critical as shown in a previous work [6]; the hardness of the material does not significantly change after pre-aging for at least three weeks and one week of natural aging before paint-bake does not have a significant influence either.

2.3. Mechanical properties

Vickers micro-hardness (HV0.1) was measured five times per sample using a load of 100 g. Tensile tests were conducted using a Bähr DIL 805 A/D deformation dilatometer (similarly as reported in [4,5]) at a strain rate of 0.006 s^{-1}. Four specimens were used for all conditions, cut parallel to the rolling direction. The specimens were taken from parts as indicated in Figs. 3 and 4a.

Warm tensile tests were performed in triplicate with equal parameters as above after inductively heating the samples at 20 K s^{-1}. Deformation was started 30 s after the beginning of heating as shown in Fig. 4 b. These parameters were chosen to simulate heating of the blank in the blank holder (*cf.* Fig. 6b "fringe area"). The heating rate was controlled by a thermocouple soldered to the reduced section of the tensile specimen (Fig. 4). Warm tensile tests were conducted at strain rates of 0.006 s^{-1} and 1 s^{-1} aiming at evaluating the strain rate sensitivity. Strain measurement was accomplished using quartz push rods hooked to the shoulders of the tensile speciments and connected to a linear variable differential transformer (LVDT). A photograph of the setup is given in Fig. 4.

2.4. Differential scanning calorimetry

Samples with a diameter of 3 mm and an average weight of 112 mg were punched from the sheet or parts (Fig. 3), deburred using sand paper and cleaned in isopropyl alcohol. They were placed in a Al_2O_3

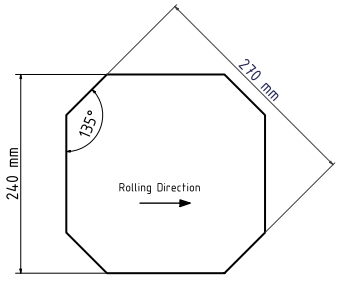

(a)

(b)

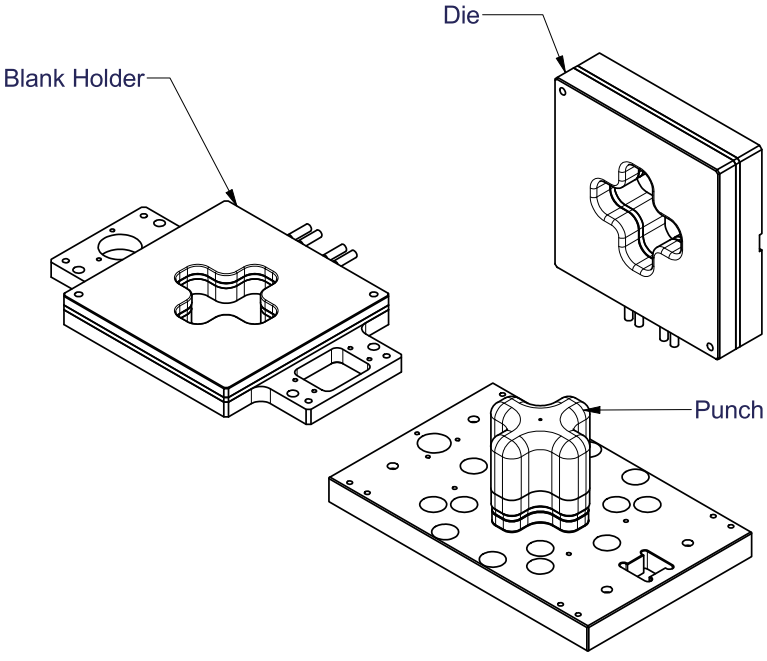

(c)

Fig. 1. (a) Blank geometry, (b) 160 t hydraulic double-sided press and (c) exploded view of cross-die deep-drawing tool.

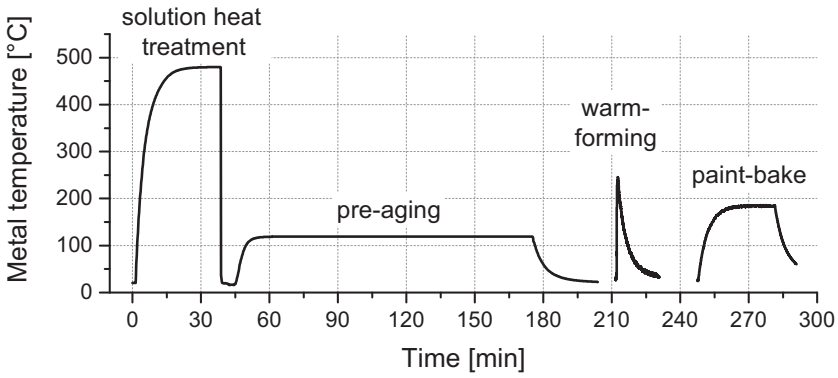

Fig. 2. Time-temperature curve of the whole process chain based on actual metal temperature measurements.

crucible and measured in a nitrogen atmosphere using a Netzsch DSC 204 F1 calorimeter at a heating rate of 10 K min^{-1} up to 600 °C. The obtained curves were baseline-corrected by fitting a third degree polynomial to the peak-free regions at 100–130 °C and 510–525 °C similar to the approach described by Osten et al. [29].

2.5. Transmission electron microscopy

For TEM, samples were ground using SiC disks with grits varying from 300 to 1200 in order to obtain thin foils with approximately 100 μm thickness. Disks with 3 mm diameter were punched from the grinded foils and electron-transparent samples were prepared *via* jet electro-polishing in a Struers Tenupol-5 with a nital electrolyte consisting of a mixture of concentrated nitric acid (33 vol%) and methanol (67 vol%) at −20 °C and 12 V. Samples were electro-polished until perforation and rinsed in three subsequent pure methanol baths before left to dry in air. A Thermo Scientific™ Talos F200X scanning transmission electron microscope (STEM) was used. The microscope operates a field-emission gun Schottky filament at 200 keV with STEM resolution better than 0.14 nm and it is equipped with four Super-X silicon drift detectors for energy dispersive X-ray spectroscopy (EDX). A high visibility double-tilt holder optimised for EDX was used.

3. Results

3.1. Stability of the pre-aged temper

The hardness trend of the pre-aged temper over the course of approximately three years is given in Fig. 5 alongside with the natural aging curve of a solution heat treated and water-quenched sample (*i.e.*, W temper developing into the T4 temper) and the T6 hardness for comparison. During our observation period of three years, the pre-aged temper increased in hardness at an apparently constant rate of 1.120×10^{-1} HV day^{-1} (Pearson $R = 0.92$). In other words, it takes approximately 84 days for the material's hardness to increase by 1 HV.

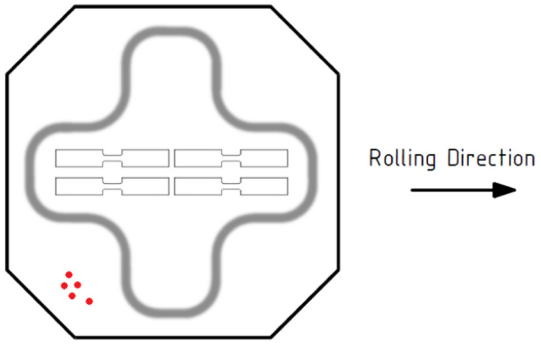

Fig. 3. Schematic top view of deep-drawn part indicating the approximate sampling locations for tensile tests and DSC (red dots).

3.2. Warm-forming behavior

Both T6 and the pre-aged temper are practically not formable by deep-drawing using the cross-form die at RT due to early cracking. However, increasing the blank holder temperature to 180–250 °C and holding the blank in the closed blank holder for 30 s prior to deep-drawing enables the production of parts as shown in Fig. 6(a). The temperature trends in regions of the blank with and without direct contact to the heated blank holder (*i.e.*, in the fringe and center regions), measured using embedded thermocouples, are given in Fig. 6(b). It can be seen that the desired forming temperature is reached within approximately 10–15 s in regions with direct contact to the blank holder. In the center region, the set temperature would be reached after approximately 90 s (data not shown) but deep-drawing was started at $t = 30$ s because the areas with highest deformation are very close to areas with direct contact to the blank holder. The temperature development in the center region could not be measured after onset of forming due to tear-off of the thermocouple. However, this temperature is expected to rise rapidly once the blank comes into contact with the heated punch. Forming is indicated by zigzag lines in Fig. 6(b).

Fig. 6(c) shows the maximum draw depths. The pre-aged temper allows for roughly 10–20% greater drawing depth compared to T6.

To further investigate the materials' behaviors at elevated temperatures, warm tensile tests were performed after heating the specimens at a similar rate as in the press and starting the deformation at t = 30 s also (compare Figs. 4b and 6b). Strength levels are reduced and elongation is generally increased for higher temperatures at a strain rate of 0.006 s^{-1} (Fig. 7a and b). At a strain rate of 1 s^{-1}, strength levels are reduced. The elongation at break is also lowered compared to RT for 120–180 °C; for the higher temperatures, elongation is generally increased (Fig. 7c and d). This effect on elongation is much stronger for T6 whereas the elongation of the pre-aged temper over temperature remains more uniform.

The pre-aged temper shows stronger strain-hardening especially at RT and up to 210 °C (Fig. 7e). The difference in strain hardening between the two tempers becomes less pronounced with increasing the temperature. Although the strain-hardening coefficient n between 3 and 6% true strain could not be calculated for 230 and 250 °C due to the early onset of necking, it can be seen from the tensile curves that the difference in strain hardening between the two tempers further decreases with temperature and eventually mostly vanishes in the tensile curves recorded at 250 °C.

In contrast to temperature, changes in strain rate appear to have little influence on the work-hardening coefficient within the investigated range (Fig. 7e).

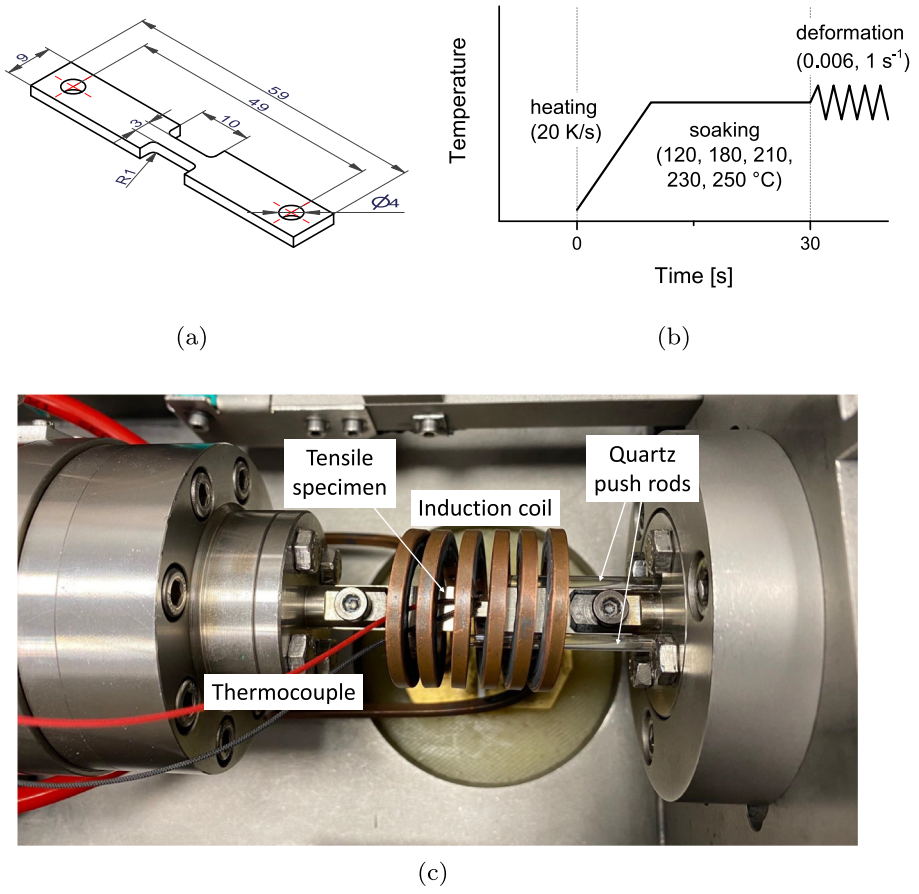

Fig. 4. (a) Tensile sample geometry (measurements in mm), (b) schematic of warm tensile testing procedure and (c) photograph of dilatometer setup.

3.3. Final mechanical properties

The mechanical properties of the paint-baked parts in comparison to the blank materials before warm-forming are given in Fig. 8. For T6 blanks, the mechanical properties of the final parts are inferior to the original temper, while for pre-aged blanks, the warm-forming and paint-bake process improves strength, yet reduces elongation. For as-received T6, the yield strength (YS) is 535 MPa and the ultimate tensile strength (UTS) is 590 MPa. Compared to the peak-aged condition (T6), paint-baked parts from T6 blanks show roughly 90% of the initial strength: The YS and UTS of the sample warm-formed at 180 °C and paint-baked (*i.e.*, the sample with the highest YS) are 468 and 538 MPa, respectively. In contrast, parts from the pre-aged blanks achieve approximately 95% of peak-aged strength: For warm-forming at 210 °C and paint-bake, the YS and UTS are 509 and 563 MPa, respectively.

For both pre-aged and T6 blanks, differences in forming temperature in the range of 180–230 °C do not significantly influence the final mechanical properties of the parts. Conversely, a forming temperature of 250 °C slightly reduces the elongation at break.

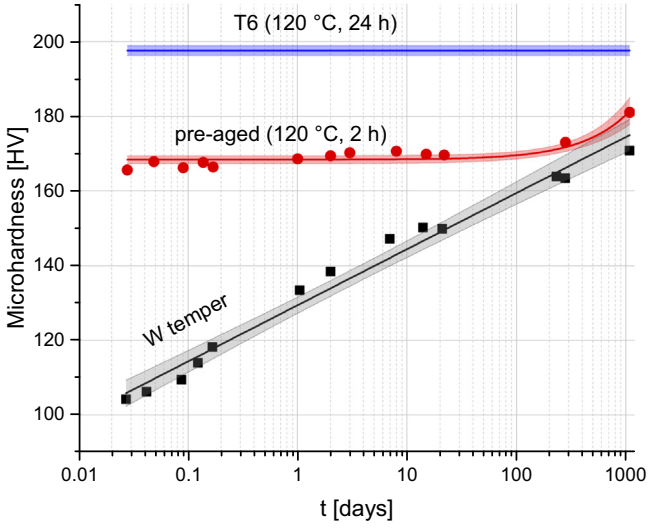

Fig. 5. Microhardness during natural aging at RT of the pre-aged temper and the W temper. T6 temper is given for comparison. The error bands represent the 95% confidence intervals of the linear and linear logarithmic fits.

3.4. DSC measurements

Fig. 9 shows the DSC curves of the material as-delivered (T6) and the pre-aged temper. Additionally, the curves of these two tempers, warm-formed at different temperatures before measurement, are also given in Fig. 9.

Peak 1 can be attributed to the dissolution of the η′ phase [30]. Since η′ is the main hardening phase in AA7075 [31], the peak is very prominent in the T6 temper. In contrast, for the pre-aged temper, peak 1 is very weak.

Peak 2 is due to the formation of the equilibrium phase η [32]. These peaks are less pronounced after warm-forming at 230 and 250 °C. The following peak, 2a, is reported as either the transformation to coarse η phase by Kumar et al. [30] or T-phase by Jiang et al. [33]. Both are not usually considered strengthening phases in AlZnMgCu alloys.

The broad endothermic event (peak 3) is due to the dissolution of the η-phase. Only the T6 samples—with and without additional

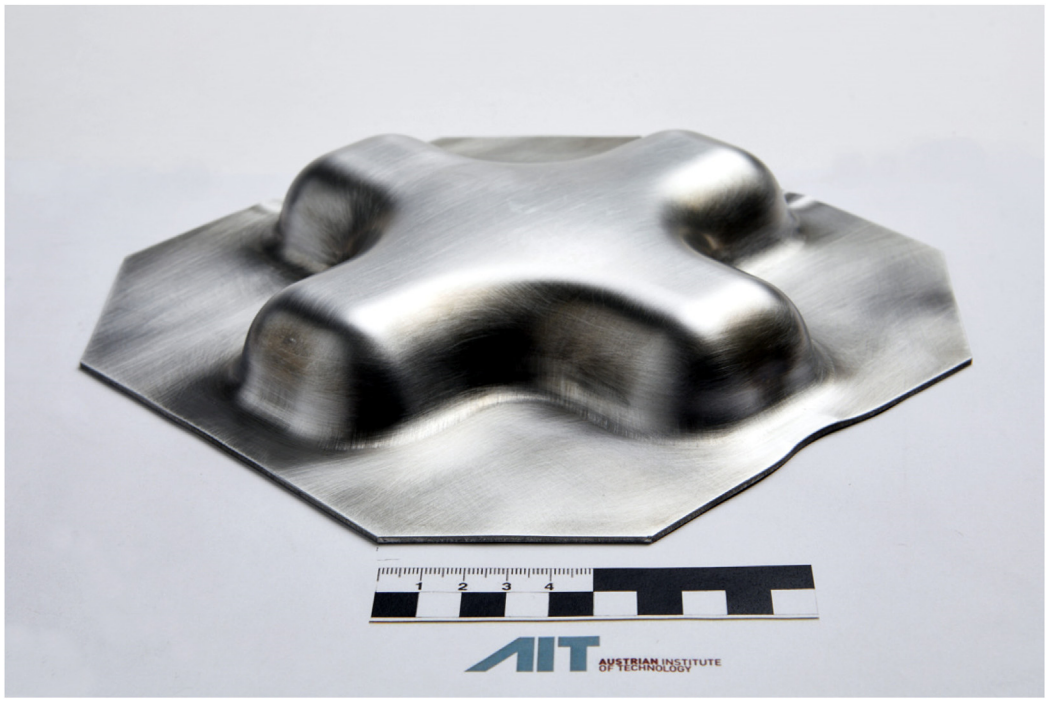

(a)

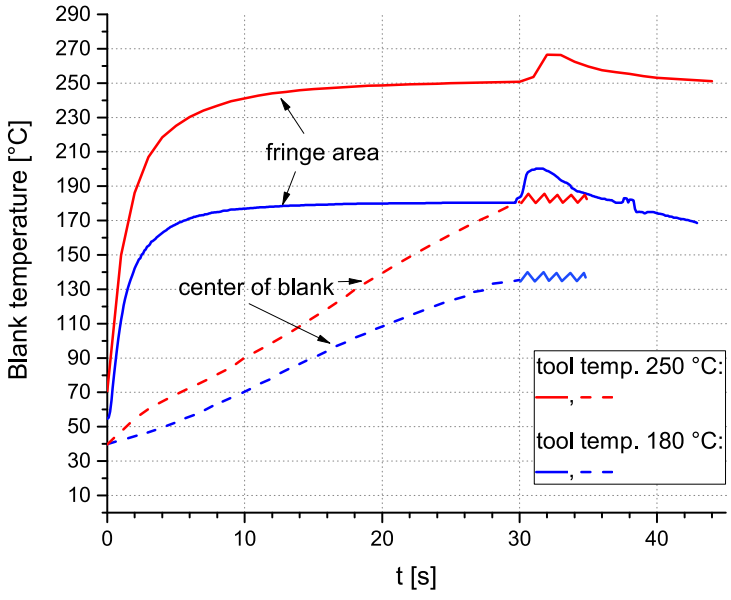

(b)

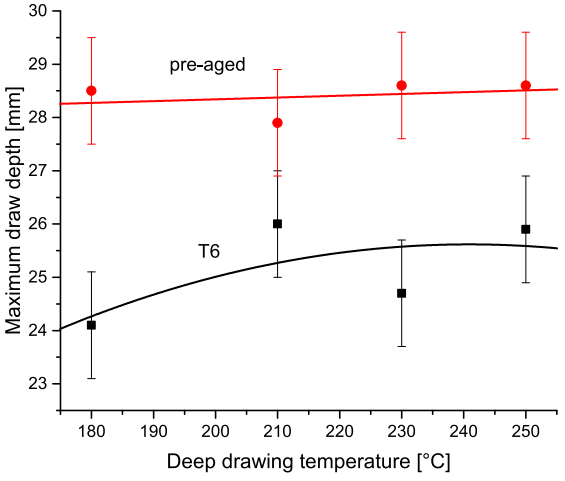

(c)

Fig. 6. (a) Deep-drawn part with a draw depth of 28.6 mm. (b) Typical temperature profile in the center and the fringe area of the blank after closing the blank holder for desired forming temperatures of 180 and 230 °C. (c) Maximum draw depth for both tempers at various temperatures. The error bars represent the minimal step size of the hydraulic press (*i.e.*, 1 mm).

warm-forming—show a further dissolution peak (4) at around 490 °C. Li et al. [34] attribute this peak to the dissolution of the S phase.

After paint-bake heat treatment (Fig. 10) the temperatures of peak 1 are much more similar between the samples, especially for the pre-aged temper. All curves show a significant decrease in peaks 2 and 2a. For the sample that was pre-aged, warm-formed at 250 °C, and paint-baked, these two peaks disappeared completely. No change can be observed for the dissolution peaks 3 and 4.

3.5. Microstructure

Figs. 11(a) and 12(a) show bright field TEM and high-angle annular dark field (HAADF) STEM, respectively, of the microstructure of a pre-aged AA7075 warm-formed at 180 °C and subsequently paint-baked. In Fig. 11(b), a corresponding selected area diffraction pattern (SADP) along the Al [001] axis is given. The extra diffraction spots are in good agreement with previous studies on η' in 7xxx series Al alloys

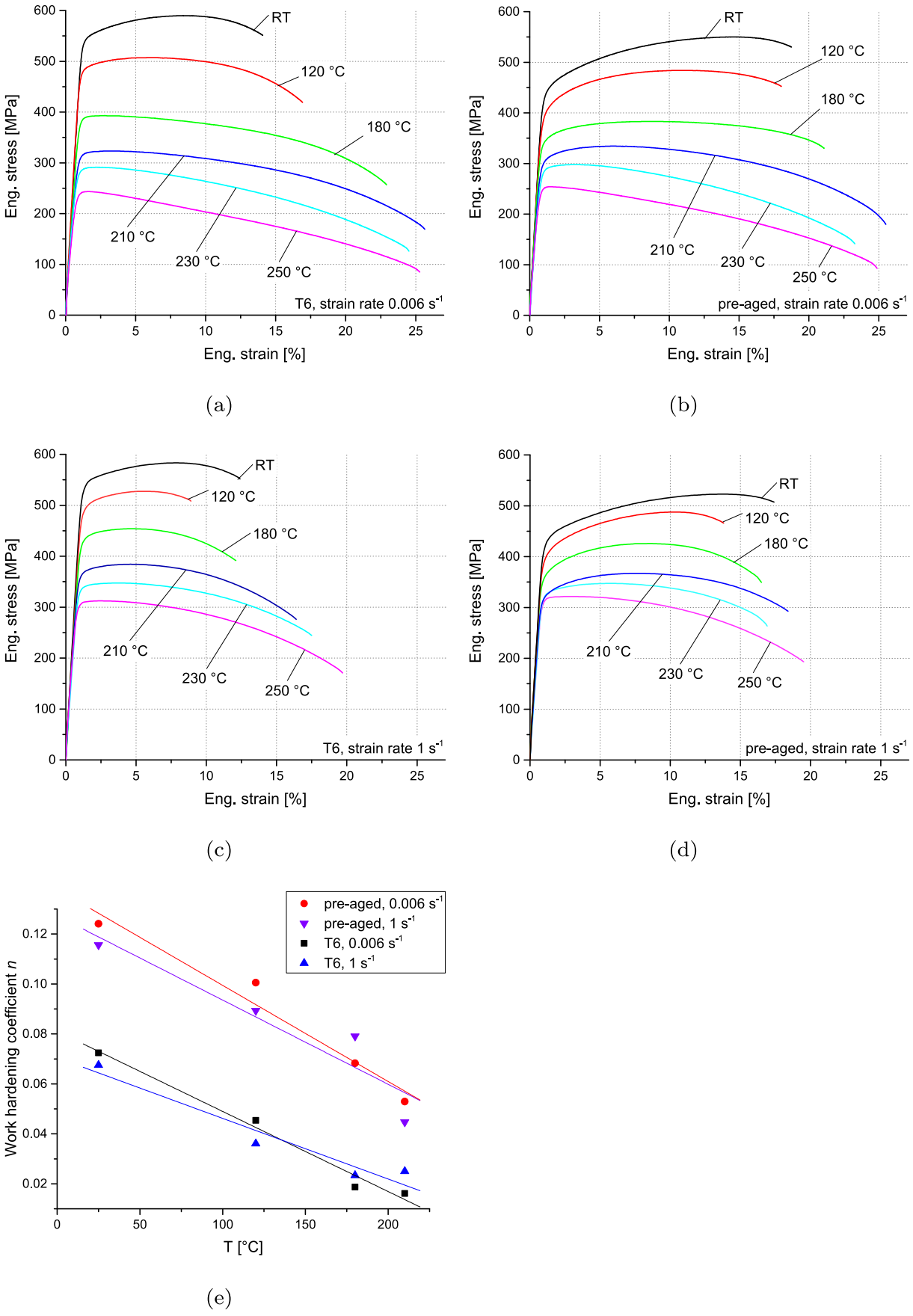

Fig. 7. Tensile curves at several temperatures for (a) T6, 0.006 s^{-1}, (b) pre-aged temper, 0.006 s^{-1}, (c) T6, 1 s^{-1}, (d) pre-aged temper, 1 s^{-1}, (e) *n*-values of the two tempers (calculated from true stress–true strain curves between 3 and 6%).

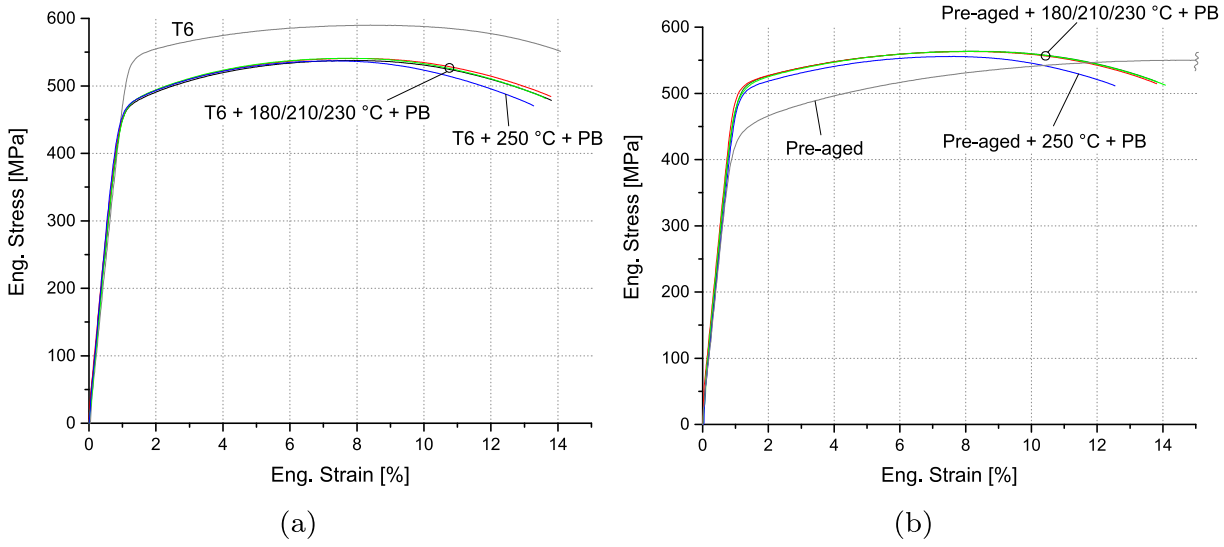

Fig. 8. Tensile curves before and after warm-forming (temperatures indicated in figure) with subsequent paint-bake (PB) heat treatment of (a) T6 and (b) pre-aged temper.

[35–37]. For comparison, a SADP of a sample warm-formed at a higher temperature of 230 °C and subsequently paint-baked is shown in Fig. 11(c). This SADP also shows the spots associated with the η′-phase.

While the majority of the phases detected were η′, we also observed potentially hardening hexagonal phases whose lattice parameters do not match with previously reported phases in the pre-aged sample warm-formed at 180 °C and subsequently paint-baked. HAADF-STEM and HRTEM micrographs along with fast Fourier transform (FFT) of such a hexagonal precipitate are given in Fig. 13.

All hardening precipitates, including the potential novel phase, are clearly identified as a Mg/Zn precipitates in Fig. 12, where a comparison of the distribution and composition of nano-scale hardening precipitates of T6 and the pre-aged, warm-formed (180 °C and 230 °C) and paint-baked samples is given (the HAADF field of view in Fig. 12a is identical to that in Fig. 13). It can be seen that the areal density of Mg/Zn precipitates is highest for T6 and the precipitates appear to be smaller and more numerous.

In Fig. 14, HAADF-STEM and EDX maps at a lower magnification are given for pre-aged AA7075 warm-formed at 180 °C and subsequently paint-baked. The EDX map for Cr identifies most of the particles as Cr-rich dispersoids (Fig. 14). Mg and Zn appear to be quite evenly distributed; however, Mg and Zn also show a tendency to precipitate at the grain boundaries and at dispersoids (Fig. 14c and d). In contrast, high Fe and Cu concentrations were only found in a fraction of the dispersoids (Fig. 14e and f).

4. Discussion

The pre-aged material can be considered stable for time frames most relevant to industrial production (*i.e.*, a few weeks) since it only exhibits a very slow and linear increase in hardness. The relative stability of the raw material allows delays between heat treatment of the blanks and the forming operation, facilitating logistics compared to W temper forming, where forming has to be performed shortly after quenching [7].

While direct conclusions from hardness measurements to the microstructure are difficult to draw, it has been suggested that a linear increase of hardness in age-hardenable Al alloys is due to short range ordering contributions. An increase in shearable obstacles would result in a relation that can be described by , where H is the hardness and f is

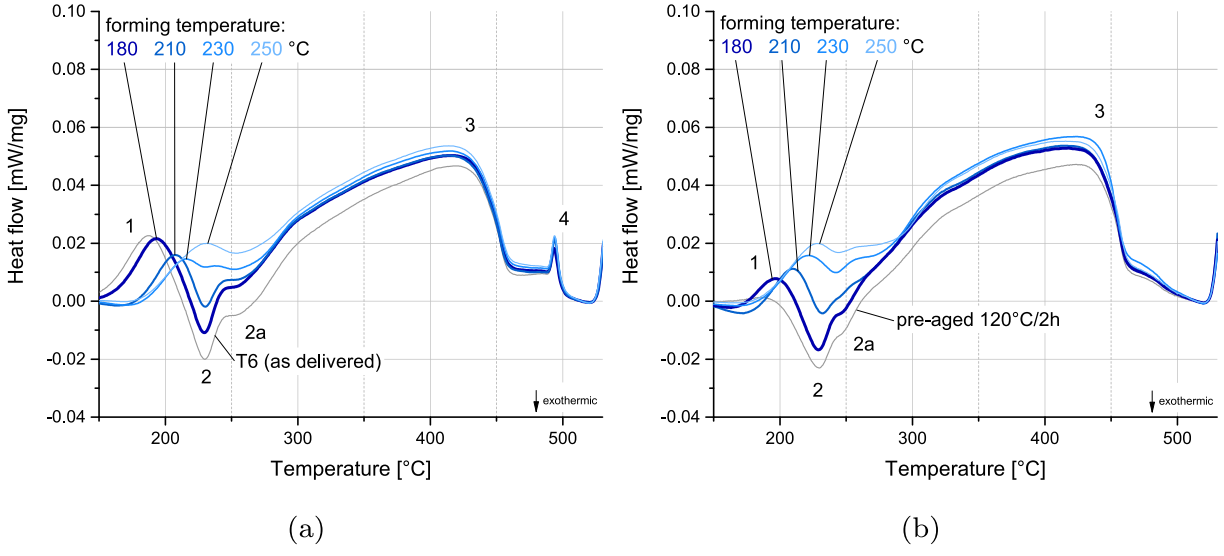

Fig. 9. DSC curves before and after warm-forming at various temperatures: (a) T6 (b) pre-aged temper. The arabic numerals correspond to the peaks mentioned in the text.

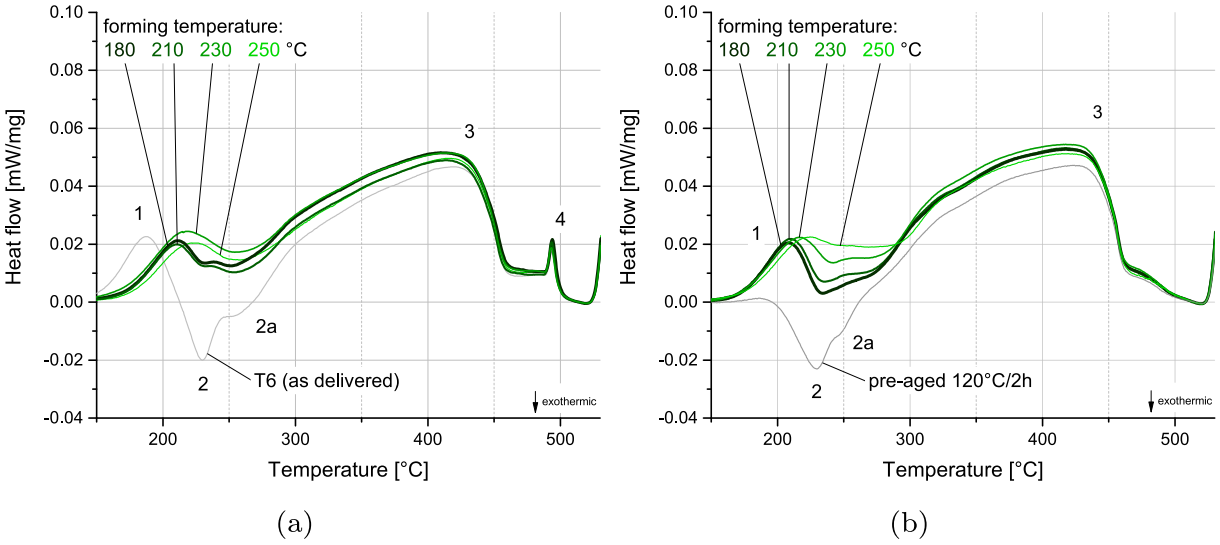

Fig. 10. DSC curves before and after warm-forming at various temperatures plus paint-bake: (a) T6 (b) pre-aged temper. The arabic numerals correspond to the peaks mentioned in the text.

the volume fraction of obstacles [38–40]. Therefore, it can be concluded that the secondary aging of the pre-aged material at RT occurs in the coherent regime by formation of clusters and GP-zones. [41]

Inevitably, the use of T6 blanks for warm-forming with subsequent paint-bake leads to overaging, explaining the lower mechanical properties. The contribution of the warm-forming step to over-aging can be

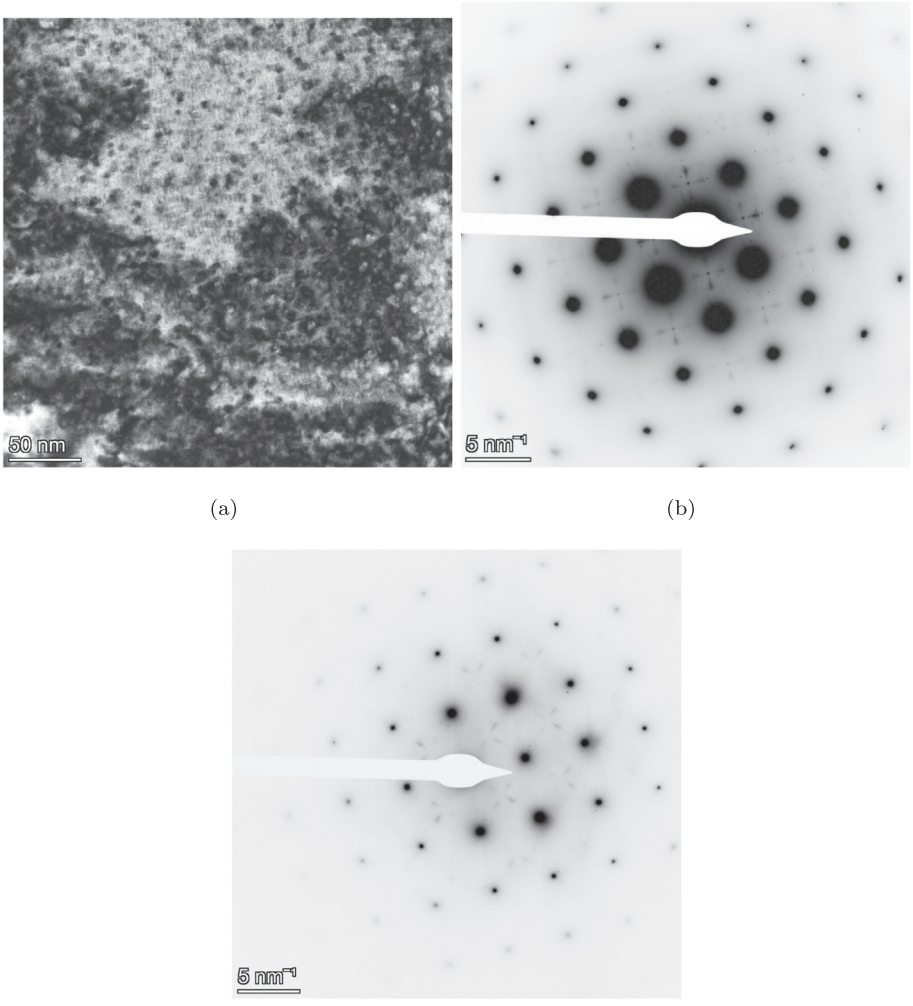

Fig. 11. (a) TEM bright field overview of hardening precipitates of pre-aged AA7075 warm-formed at 180 °C and subsequently paint-baked, (b) selected area diffraction pattern along the [001] axis, corresponding to (a), and (c) selected area diffraction pattern along the [001] axis of pre-aged AA7075 warm-formed at 230 °C and subsequently paint-baked.

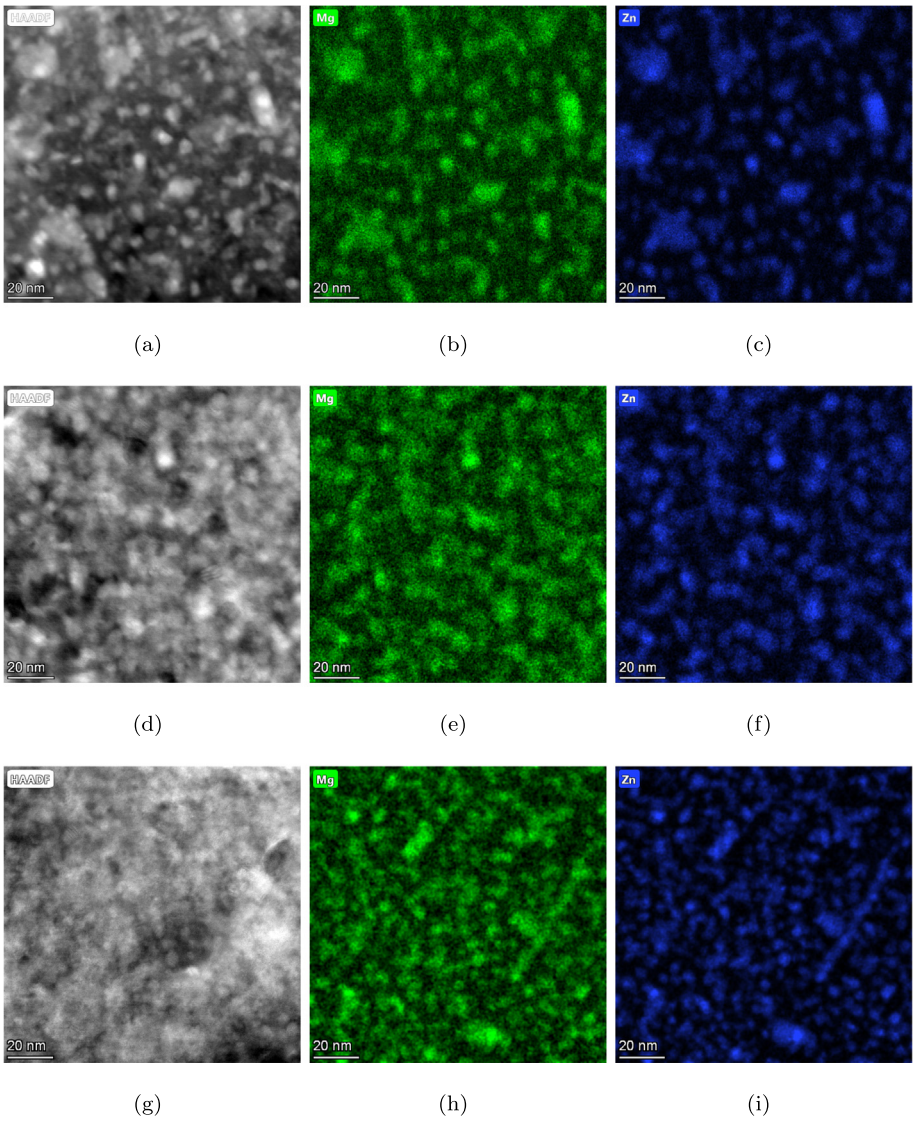

Fig. 12. HAADF-STEM and EDX maps of (a, b, c) pre-aged AA7075 warm-formed at 180 °C and subsequently paint-baked and (d, e, f) pre-aged AA7075 warm-formed at 230 °C and subsequently paint-baked, and (g, h, i) AA7075 T6 (as delivered).

seen in the DSC curves in Fig. 9(a): For the lower forming temperatures of 180 °C and 210 °C, peak 1, which is potentially associated with the dissolution of the η′ phase, shifts to the right compared to T6. Peak 2, potentially due to the precipitation of η, is attenuated. This can be interpreted as a coarsening of η′ and a simultaneous reduction of matrix supersaturation. For the highest forming temperature of 250 °C, peak 1 disappears completely and peak 2 becomes endothermic. This change in peaks could indicate that η′ has been converted into η. The curve of the sample formed at 230 °C lies between these two phenomena.

Similar observations can be made for the pre-aged and warm-formed samples (Fig. 9b). However, in contrast to T6, the initial pre-aged material is under-aged. Its DSC curve hardly shows an η′ peak which is in agreement with the findings of Lee et al. [16] who found a fine distribution of predominant GP-zones after pre-aging at 120 °C for 2 h. The warm-forming, however, already leads to the formation of η′ as evidenced by the appearance of peak 1. The potential S phase peak (peak 4 in Figs. 9a and 10a) was absent for all samples made from our pre-aged blanks. This can be interpreted to mean that the S-phase was completely dissolved by our solution heat treatment and not re-precipitated due to the high cooling rate during quenching in water.

While the DSC curves of the warm-formed samples before paint-bake differ significantly for the various forming temperatures, the curves are much more uniform after paint-bake (Fig. 10). This is especially true for the samples made from T6 blanks, for which peak 2 (precipitation of η) has strongly weakened or disappeared. The curves of the samples made from pre-aged blanks still show greater variety and, for the lower warm-forming temperatures (180–210 °C), a stronger exothermic dip in the same region as peak 2. This could indicate that, due to the underaged starting material and the low warm-forming temperatures, the formation of η (*i.e.*, overaging) has not occured to the same extent as in the other samples. Lang et al. [42] found the transition from η′ to η to occur around 230 °C. However, we found η′ to be the predominant hardening phase in pre-aged samples warm-formed at 230 °C and paint-baked as well.

Despite the DSC curves being much more uniform after paint-bake, the effect of the warm forming temperatures on the temperature of peak 1 is still visible. This can be correlated to coarsening of the η′ phase [24,30] or transformation to η.

For both T6 and the pre-aged material, the influence of non-shearable particles on work-hardening during warm-forming can be expected to be minor because the shearable–non-shearable transition of

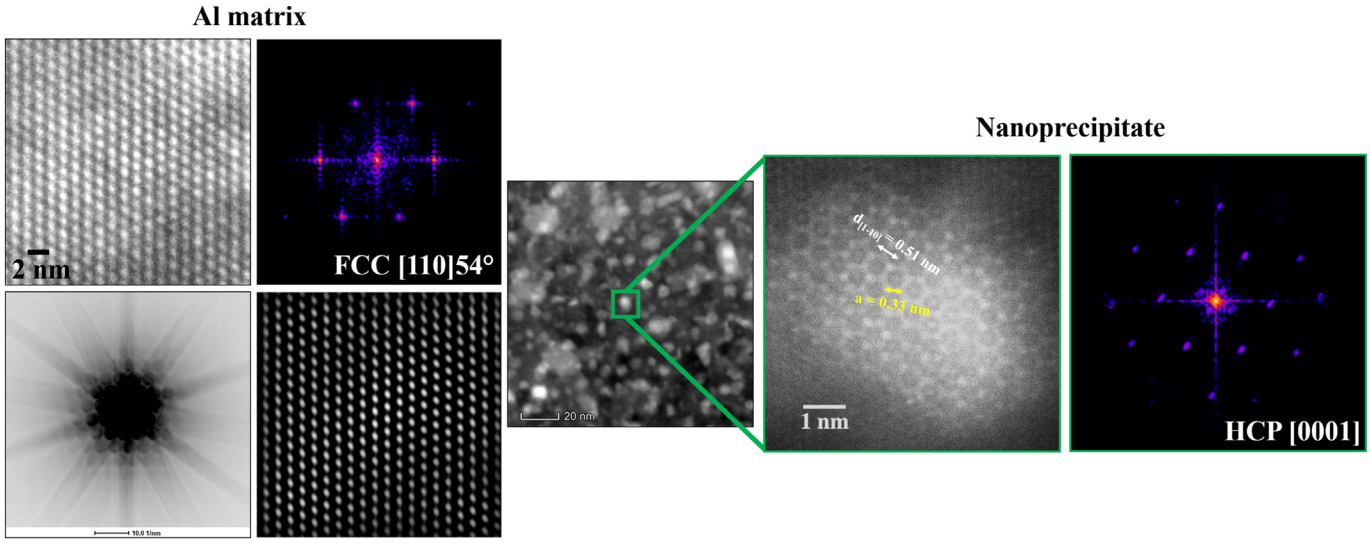

Fig. 13. High-magnification HAADF micrograph of AA7075 warm-formed at 180 °C and subsequently paint-baked, showing two areas of interest: HRSTEM micrographs of the Al matrix oriented along the [110] axis and the observed hexagonal nanoprecipitate along [001] with their respective FFT.

hardening precipitates generally only occurs upon overaging [43] and the direct influence of Cr-rich dispersoids on the mechanical properties is usually small [44]. In addition, the number density and size distribution of dispersoids in both tempers can be expected to be essentially the same because the solution heat treatment time is too short to have significant influence on the dispersoid distribution in sheet material. Therefore, the pronounced differences in strain hardening between the two tempers (Fig. 7 e) are more likely a result of dislocation storage due to trapping of mobile dislocations by other dislocations or differences in the dynamic recovery rate.

A main difference between the T6 temper and the pre-aged temper is the higher super saturated solute content of the latter. It is well known that the dynamic recovery rate is strongly influenced by solute content [45]. One reason for the reduction of the dynamic recovery rate with increasing solute content is that solutes lower the stacking-fault energy, restricting cross-slip [44]. At higher temperatures, higher diffusion rates favor dynamic recovery and the differences in strain hardening between the tempers are less pronounced (Fig. 7e).

Both investigated tempers show some strain rate sensitivity at elevated temperature: The elongation at break is reduced while YS and UTS are increased at the higher strain rate (Fig. 7). These effects, in particular the reduction in elongation at break, appear to be much stronger in the T6 condition compared to the pre-aged temper. Furthermore, in T6, the reduction in elongation at the higher strain rates is most pronounced for relatively low temperatures of 120 °C up to roughly 210 °C. Warm deformation leads to a complex interplay of various microstructural mechanisms; to explain the observed strain rate sensitivity, two effects can be considered especially important: First, at higher strain rates, the material has less time to undergo dynamic recovery. Secondly, dissolution, precipitation and growth of second phase particles are reduced for the same reason. [46] Such dissolution and coarsening of hardening precipitates may be a possible explanation for the lower stress levels and higher elongation of T6 at low strain rates. Likewise, for high strain rates, temperatures above roughly 210 °C improve formability. These temperature effects are enhanced by the soaking period before deformation (Fig. 4c). In contrast, the pre-aged temper is underaged and precipitation processes may be favored over dissolution and coarsening.

With respect to the warm-forming behavior, a remarkable finding is that the maximum draw depth of the pre-aged blanks is approximately constant over the investigated temperature range (Fig. 6c) despite the different tensile behavior (Fig. 7). In the warm tensile tests, the strain levels drop and elongation in most cases increases at higher temperatures but the pronounced strain-hardening also disappears. Strain hardening prevents early necking in the tensile test as well as excessive thinning in deep-drawing [47]. Therefore, the positive effects of lower stress levels and higher elongation on formability may be counteracted by stronger thinning due to lower strain hardening, resulting in an overall constant maximum draw depth.

In addition, for the pre-aged temper, the elongation at break only significantly rises with temperature at the low strain rate while it remains roughly in the same range as at RT for the high strain rate. Cracks form first in regions with high deformation and, hence, relatively high strain rates. This could be an explanation for the approximately constant draw depth of the pre-aged temper. In contrast, the elongation of T6 rises strongly with temperature starting at roughly 180 and 210 °C for both the slow and faster strain rate, respectively. This could be due to dissolution of existing hardening phases as evidenced by peak 1 in Fig. 9(a) and explain why draw depth rises with temperature for T6.

Overall, the findings regarding strain rate sensitivity suggest that slow forming speeds are beneficial for warm-forming of AA7075 in the investigated tempers. This is in agreement with our preliminary forming trials that led us to fix the speed at relatively slow 5 mm/s. Further research could aim to find the best process parameters for increased forming speed.

The overall microstructure of the pre-aged, warm-formed at 180 °C, and paint-baked parts appears similar to that of the pre-aged sample warm-formed at 230 °C and paint-baked (Fig. 12a–f) in STEM analysis. The microstructures are comparable to T6 (Fig. 12g–i). This is in good agreement with Lee et al. [16] who found that pre-aging in combination with paint-bake can lead to a very fine distribution of hardening precipitates. However, the distribution of hardening precipitates in T6 is even more favorable: T6 appears to contain a high number of very small hardening precipitates (Fig. 12b–d). This fine distribution is also indicated by a lower temperature of peak 1 in the DSC curves (Fig. 10) and the slightly higher strength of T6. While the majority of hardening phases found in pre-aged, warm-formed at 180 °C, and paint-baked sample were η′ (*cf.* Fig. 11b), further work is required to establish the structure of the precipitate given in Fig. 13.

The precipitate distribution of parts made by warm-forming T6 blanks and subsequent paint-baking is expected to be coarser than for samples made from pre-aged blanks due to over-aging. This coarsening is evidenced by the shift of peak 1 to higher temperatures in the DSC curves (Fig. 10).

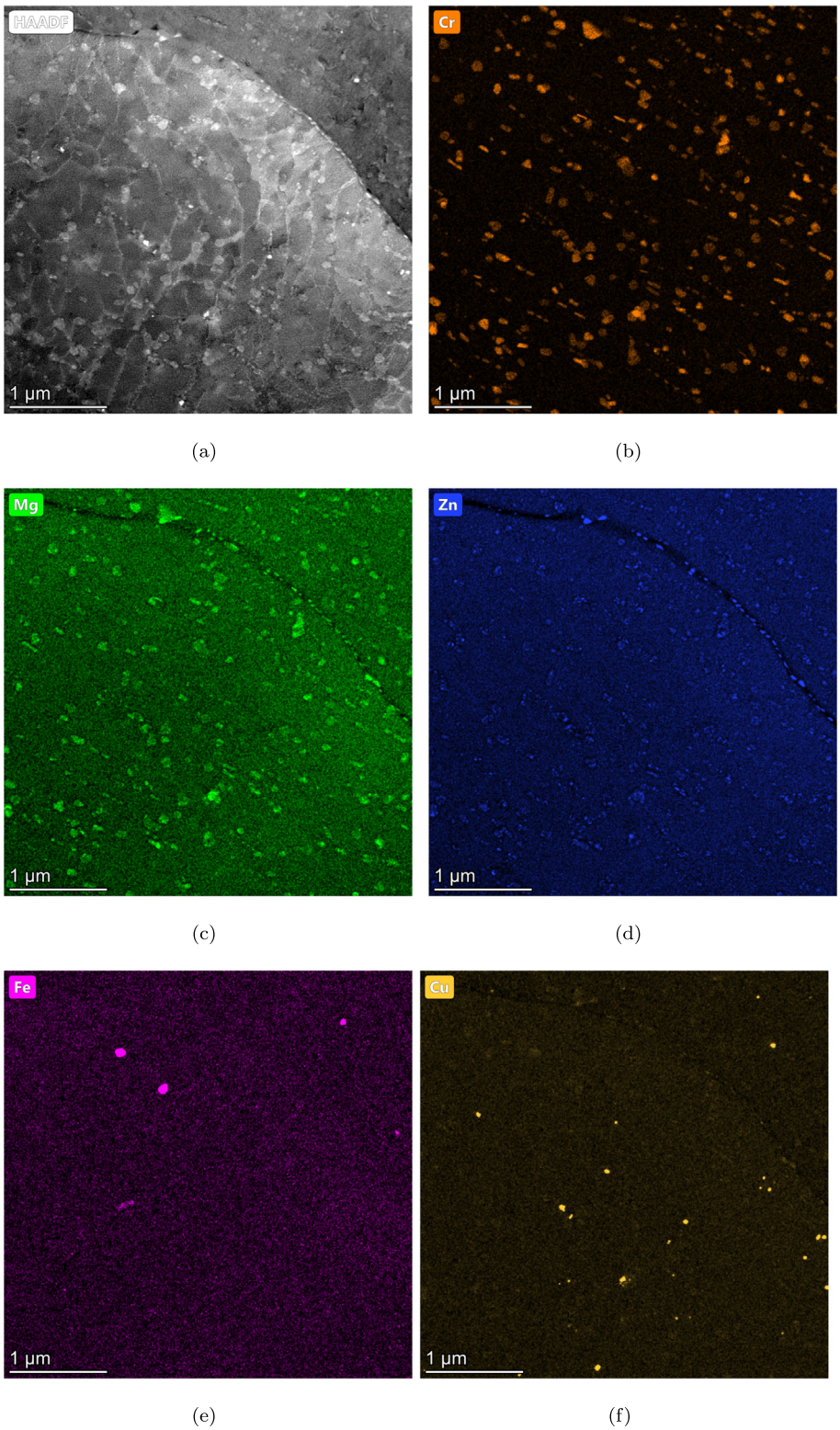

Fig. 14. Pre-aged AA7075 warm-formed at 180 °C and subsequently paint-baked: (a) HAADF-STEM and (b, c, d, e, f) EDX.

Using EDX in STEM, the disconnected precipitates at the grain boundaries of the pre-aged, warm-formed (180 °C) and paint-baked sample were found to be Zn-rich (Fig. 14), like equilibrium η precipitates. In contrast to continuous η precipitates at the grain boundaries, discontinuous η phases are thought to be effective in preventing intergranular corrosion and improve fracture toughness [48]. Slow quenching rates after solution heat treatment, overaging, or retrogression and re-aging (RRA) can be used to generate such a microstructure [49,50]. RRA is also aimed to increase the Cu content of grain boundary precipitates in order to reduce galvanic interaction with the matrix [51]; yet we found Cu predominantly in some of the intragranular precipitates. Further research on the influences of quenching rate, pre-aging, warm-forming, and paint-bake on corrosion behavior is recommended.

The strength of the pre-aged, warm-formed, and paint-baked parts is only roughly 5% lower than that of T6 (Fig. 8). This means that pre-aging AA7075 at 120 °C can not only improve the paint-bake response, but can also be leveraged for an additional forming step. As previously reported [6,15,16], the probable mechanism is the formation of thermally stable GP-zones that act as nuclei for the precipitation of η'. The usable forming temperature is therefore limited by the stability of these GP zones. A decline in mechanical properties occurs when a warm-forming temperature of 250 °C is used. Comparing our results to the previous works [6,15,16], the deformation of the material during deep-drawing does not seem to have significant influence on the efficacy of the pre-aging approach for improving paint-bake response.

Interestingly, the same upper temperature limit applies to the T6 blanks: A warm-forming temperature of 250 °C resulted in poorer mechanical properties after paint-bake. During RRA treatments of AA7075, similar temperatures are used for the retrogression step. While re-aging at 120 °C can fully restore T6 strength, paint-baking cannot [12]. Re-aging at 120 °C can re-precipitate the fine precipitates needed for peak strength whereas paint-baking can only do so partially and with the help of surviving nuclei. Therefore, warm-forming temperatures and times that lead to extensive retrogression should be avoided also when using T6 blanks. This is in agreement with the findings reported by Huo et al. [24], who found excessive precipitate coarsening at high warm-forming temperatures and suggested an optimum warm-forming temperature of 200 °C for T6 blanks.

Another important factor in warm and hot forming is the lubricant. While the results reported here were achieved with a solid dispersion lubricant (Molyduval Moralub FB 100 Z), also suitable for hot stamping, the use of oil-based lubricants is preferred by the automotive industry due to reduced cleaning costs. However, oil-based sheet lubricants have a thermal stability of typically up to roughly 220 °C which makes them unsuitable for hot-stamping. In the warm-forming process, however, oil-based lubricants may be used. We performed limited experiments using T6 blanks and an oil-based lubricant (Zeller + Gmelin Multidraw Drylube E 1). We found it suitable for warm-forming at 180–210 °C but the achievable maximum draw depth was roughly 10% less than using the solid dispersion lubricant due to greater friction. However, further optimization may help to overcome this limitation.

5. Conclusions

We proposed a warm-forming process that consists of pre-aging AA7075 at 120 °C for 2 h, deep-drawing at a temperature of 180–210 °C, and a simulated paint-bake treatment. The strength of the produced parts was roughly 95% of T6. The good paint-bake response is due to the formation of thermally stable GP-zones during pre-aging, which can survive the warm-forming process and act as nuclei for the precipitation of hardening phases during paint-bake or even during the warm-forming process itself. Compared to the use of T6 blanks, negative effects of over-aging are mitigated.

The maximum draw depth of the pre-aged blanks was higher than for T6 blanks at all temperatures between 180 and 250 °C. Despite different tensile behavior at various temperatures within this range, the maximum draw depth of the pre-aged blanks did not change significantly with temperature. In contrast, the maximum draw depth of T6 blanks increased with temperature. We ascribe this divergent deep-drawing behavior to differences in strain hardening and strain rate sensitivity between the two tempers.

Since the pre-aging can be performed already at the rolling plant, the warm-forming process facilitates logistics and reduces equipment requirements at the automaker where no solution heat treatment is needed. In addition, the lower temperatures allow the use of oil-based lubricants.

Electron microscopy investigation of a pre-aged, warm-formed, and paint-baked sample revealed a potentially hardening Mg- and Zn-rich phase with HCP structure. The estimated lattice parameters ($a = 0.33$ nm, $d_{[1-10]} = 0.51$ nm) did not match with previously reported phases in the alloy system.

CRediT authorship contribution statement

Johannes A. Österreicher: Conceptualization, Writing - original draft, Investigation, Data curation.**Matheus A. Tunes:**Investigation.**Florian Grabner:**Investigation, Data curation.**Aurel Arnoldt:**Investigation, Visualization.**Thomas Kremmer:**Investigation.**Stefan Pogatscher:**Conceptualization, Project administration, Supervision.**Carina M. Schlögl:** Conceptualization, Project administration, Supervision.

Declaration of competing interest

The authors declare that they have no known competing financial interests or personal relationships that could have appeared to influence the work reported in this paper.

Acknowledgements

This work received support from the Austrian Research Promotion Agency (FFG) in the projects 3DnanoAnalytics (FFG-no. 858040) and AMALFI (FFG-no. 872641) as well as by the Austrian Institute of Technology (independent research 2019). MAT and SP are grateful to the European Research Council (ERC) excellent science grant TRANSDESIGN through the Horizon 2020 program (contract no. 757961). The authors would like to thank Professor Peter J. Uggowitzer (ETH Zurich and MU Leoben) for fruitful discussion and the technical staff of LKR Ranshofen and MU Leoben for their invaluable assistance.

Data availability

The data related to this work can be obtained from the corresponding author upon reasonable request.

References

[1] A. Afseth, Ultra-high-strength aluminium alloys — vehicle production's next big thing, Lightw. Des. Worldw. 10 (2) (2017) 12–15, https://doi.org/10.1007/s41777-017-0002-8.
[2] N. Harrison, F. Nadeau, U. Brüx, S. Luckey, Tailored thickness hot stamping of high strength aluminum sheet, Proceedings of the 16th International Conference on Aluminum Alloys (ICAA), 2018.
[3] R. Long, E. Boettcher, D. Crawford, Current and future uses of aluminum in the automotive industry, JOM 69 (12) (2017) 2635–2639.
[4] M. Kumar, N. Ross, Influence of temper on the performance of a high-strength Al–Zn–Mg alloy sheet in the warm forming processing chain, J. Mater. Process. Technol. 231 (2016) 189–198.
[5] M. Kumar, N. Sotirov, C. Chimani, Investigations on warm forming of AW-7020-T6 alloy sheet, J. Mater. Process. Technol. 214 (8) (2014) 1769–1776.
[6] J.A. Österreicher, G. Kirov, S.S. Gerstl, E. Mukeli, F. Grabner, M. Kumar, Stabilization of 7xxx aluminium alloys, J. Alloys Compd. 740 (2018) 167–173, https://doi.org/10.1016/j.jallcom.2018.01.003.
[7] P.A. Schuster, J.A. Österreicher, G. Kirov, C. Sommitsch, O. Kessler, E. Mukeli, Characterisation and comparison of process chains for producing automotive structural parts from 7xxx aluminium sheets, Metals 9 (3) (2019) 305.
[8] N.-H. Hoang, O. Hopperstad, M. Langseth, I. Westermann, Failure of aluminium self-piercing rivets: an experimental and numerical study, Mater. Des. 49 (2013) 323–335.
[9] X. Liu, Y.C. Lim, Y. Li, W. Tang, Y. Ma, Z. Feng, J. Ni, Effects of process parameters on friction self-piercing riveting of dissimilar materials, J. Mater. Process. Technol. 237 (2016) 19–30.
[10] M. Jäckel, T. Grimm, R. Niegsch, W.-G. Drossel, Overview of current challenges in self-pierce riveting of lightweight materials, Multidisciplinary Digital Publishing Institute Proceedings, vol. 2/8, 2018, p. 384.
[11] N.R. Harrison, S.G. Luckey, B. Cappuccilli, G. Kridli, Paint bake influence on AA7075 and AA7085, Tech. rep. SAE Technical Paper, 2017.
[12] T.A. Ivanoff, J.T. Carter, L.G. Hector, E.M. Taleff, Retrogression and reaging applied to warm forming of high-strength aluminum alloy AA7075-T6 sheet, Metall. Mater. Trans. A 50 (3) (2019) 1545–1561.
[13] L. Stemper, B. Mitas, T. Kremmer, S. Otterbach, P.J. Uggowitzer, S. Pogatscher, Age-hardening of high pressure die casting AlMg alloys with Zn and combined Zn and Cu additions, Mater. Des. 181 (2019), 107927. .

[14] I. Kirman, The relation between microstructure and toughness in 7075 aluminum alloy, Metall. Trans. 2 (7) (1971) 1761–1770.
[15] K. Omer, A. Abolhasani, S. Kim, T. Nikdejad, C. Butcher, M. Wells, S. Esmaeili, M. Worswick, Process parameters for hot stamping of AA7075 and D-7xxx to achieve high performance aged products, J. Mater. Process. Technol. 257 (2018) 170–179.
[16] Y.-S. Lee, D.-H. Koh, H.-W. Kim, Y.-S. Ahn, Improved bake-hardening response of Al-Zn-Mg-Cu alloy through pre-aging treatment, Scr. Mater. 147 (2018) 45–49, https://doi.org/10.1016/j.scriptamat.2017.12.030.
[17] M. Geiger, M. Merklein, Sheet metal forming — a new kind of forge for the future, Key Engineering Materials, vol. 344, Trans Tech Publ 2007, pp. 9–20.
[18] A. A. M. Smeyers, S. Khosla, Production of formed automotive structural parts from AA7xxx-series aluminium alloys, uS Patent App. 14/424,327 (Aug. 6, 2015).
[19] E. Sáenz de Argandoña, L. Galdos, R. Ortubay, J. Mendiguren, X. Agirretxe, Room temperature forming of AA7075 aluminum alloys: W-temper process, Key Engineering Materials, vol. 651, Trans Tech Publ 2015, pp. 199–204.
[20] M. Kumar, G. Kirov, F. Grabner, E. Mukeli, Sheet forming processes for AW-7xxx alloys: relevant process parameters, Materials Science Forum, vol. 879, Trans Tech Publ 2017, pp. 1036–1042.
[21] Z. Zhang, J. Yu, D. He, Influence of contact solid-solution treatment on microstructures and mechanical properties of 7075 aluminum alloy, Mater. Sci. Eng. A 743 (2019) 500–503.
[22] M. Kumar, N. Sotirov, C. Chimani, Characterization of high strength Al-Zn-Mg alloy sheet for hot stamping, Materials Science Forum, vol. 794, Trans Tech Publ 2014, pp. 796–801.
[23] M.-Y. Lee, S.-M. Sohn, C.-Y. Kang, D.-W. Suh, S.-Y. Lee, Effects of pre-treatment conditions on warm hydroformability of 7075 aluminum tubes, J. Mater. Process. Technol. 155 (2004) 1337–1343.
[24] W. Huo, L. Hou, Y. Zhang, J. Zhang, Warm formability and post-forming microstructure/property of high-strength AA 7075-T6 Al alloy, Mater. Sci. Eng. A 675 (2016) 44–54.
[25] N. Sotirov, P. Simon, C. Chimani, D. Uffelmann, C. Melzer, Warm deep drawability of peak-aged 7075 aluminium sheet alloy, Key Engineering Materials, vol. 504, Trans Tech Publ 2012, pp. 955–960.
[26] K. Rader, T. Ivanoff, H. Shin, J. Carter, L. Hector, E. Taleff, Determining a retrogression heat treatment to apply during warm forming of a high strength aluminum AA7075 sheet material, TMS Annual Meeting & Exhibition, Springer 2018, pp. 241–246.
[27] K.E. Rader, M.B. Schick, J.T. Carter, L.G. Hector, E.M. Taleff, Conditions for retrogression forming aluminum AA7075-T6 sheet, in: C. Chesonis (Ed.), Light Metals 2019, Springer, Cham 2019, pp. 187–191, https://doi.org/10.1007/978-3-030-05864-7_25.
[28] B. Milkereit, M. Österreich, P. Schuster, G. Kirov, E. Mukeli, O. Kessler, Dissolution and precipitation behavior for hot forming of 7021 and 7075 aluminum alloys, Metals 8 (7) (2018) 531.
[29] J. Osten, B. Milkereit, C. Schick, O. Kessler, Dissolution and precipitation behaviour during continuous heating of Al–Mg–Si alloys in a wide range of heating rates, Materials 8 (5) (2015) 2830–2848.
[30] M. Kumar, AW-7075-T6 sheet for shock heat treatment forming process, Trans. Nonferrous Metals Soc. China 27 (10) (2017) 2156–2162.
[31] M. Chemingui, R. Ameur, V. Optasanu, M. Khitouni, DSC analysis of phase transformations during precipitation hardening in Al–Zn–Mg alloy (7020), J. Therm. Anal. Calorim. 136 (2019) 1887–1894, https://doi.org/10.1007/s10973-018-7856-9.
[32] X. Li, M.J. Starink, Analysis of precipitation and dissolution in overaged 7xxx aluminium alloys using DSC, Mater. Sci. Forum 331–337 (2000) 1071–1076.
[33] X. Jiang, J. Tafto, B. Noble, B. Holme, G. Waterloo, Differential scanning calorimetry and electron diffraction investigation on low-temperature aging in Al-Zn-Mg alloys, Metall. Mater. Trans. A 31 (2) (2000) 339–348.
[34] X. Li, M. Starink, DSC study on phase transitions and their correlation with properties of overaged Al-Zn-Mg-Cu alloys, J. Mater. Eng. Perform. 21 (6) (2012) 977–984.
[35] K. Stiller, P. Warren, V. Hansen, J. Angenete, J. Gjønnes, Investigation of precipitation in an Al–Zn–Mg alloy after two-step ageing treatment at 100 and 150 °C, Mater. Sci. Eng. A 270 (1) (1999) 55–63.
[36] T. Engdahl, V. Hansen, P. Warren, K. Stiller, Investigation of fine scale precipitates in Al–Zn–Mg alloys after various heat treatments, Mater. Sci. Eng. A 327 (1) (2002) 59–64, https://doi.org/10.1016/S0921-5093(01)01876-7.
[37] G. Sha, A. Cerezo, Early-stage precipitation in Al–Zn–Mg–Cu alloy (7050), Acta Mater. 52 (15) (2004) 4503–4516, https://doi.org/10.1016/j.actamat.2004.06.025.
[38] P. Dumitraschkewitz, S.S. Gerstl, L.T. Stephenson, P.J. Uggowitzer, S. Pogatscher, Clustering in age-hardenable aluminum alloys, Adv. Eng. Mater. 20 (10) (2018), 1800255. .
[39] M. Starink, L. Cao, P. Rometsch, A model for the thermodynamics of and strengthening due to co-clusters in Al–Mg–Si-based alloys, Acta Mater. 60 (10) (2012) 4194–4207, https://doi.org/10.1016/j.actamat.2012.04.032.
[40] S. Esmaeili, D. Lloyd, W. Poole, Modeling of precipitation hardening for the naturally aged Al-Mg-Si-Cu alloy aa6111, Acta Mater. 51 (12) (2003) 3467–3481, https://doi.org/10.1016/S1359-6454(03)00167-8.
[41] C.E. Macchi, A. Somoza, A. Dupasquier, I. Polmear, Secondary precipitation in Al–Zn–Mg–(Ag) alloys, Acta Mater. 51 (17) (2003) 5151–5158, https://doi.org/10.1016/S1359-6454(03)00364-1.
[42] P. Lang, T. Wojcik, E. Povoden-Karadeniz, A. Falahati, E. Kozeschnik, Thermo-kinetic prediction of metastable and stable phase precipitation in Al–Zn–Mg series aluminium alloys during non-isothermal DSC analysis, J. Alloys Compd. 609 (2014) 129–136.
[43] W. Poole, X. Wang, D. Lloyd, J. Embury, The shearable–non-shearable transition in Al–Mg–Si–Cu precipitation hardening alloys: implications on the distribution of slip, work hardening and fracture, Philos. Mag. 85 (26–27) (2005) 3113–3135.
[44] H. Zhong, P.A. Rometsch, L. Cao, Y. Estrin, The influence of Mg/Si ratio and Cu content on the stretch formability of 6xxx aluminium alloys, Mater. Sci. Eng. A 651 (2016) 688–697.
[45] I. Westermann, K.O. Pedersen, T. Furu, T. Børvik, O.S. Hopperstad, Effects of particles and solutes on strength, work-hardening and ductile fracture of aluminium alloys, Mech. Mater. 79 (2014) 58–72.
[46] J. Lu, Y. Song, L. Hua, K. Zheng, D. Dai, Thermal deformation behavior and processing maps of 7075 aluminum alloy sheet based on isothermal uniaxial tensile tests, J. Alloys Compd. 767 (2018) 856–869.
[47] J. Winklhofer, G. Trattnig, C. Lind, C. Sommitsch, H. Feuerhuber, Process simulation of aluminium sheet metal deep drawing at elevated temperatures, AIP Conference Proceedings, vol. 1252, AIP 2010, pp. 927–934.
[48] C. Qin, G. Gou, X. Che, H. Chen, J. Chen, P. Li, W. Gao, Effect of composition on tensile properties and fracture toughness of Al–Zn–Mg alloy (A7N01S-T5) used in high speed trains, Mater. Des. 91 (2016) 278–285.
[49] D. Yuan, K. Chen, L. Zhou, J. Chang, L. Huang, Y. Yi, et al., Enhancing stress corrosion cracking resistance of low Cu-containing Al-Zn-Mg-Cu alloys by slow quench rate, Mater. Des. 164 (2019), 107558. .
[50] Y.-P. Xiao, Q.-L. Pan, W.-B. Li, X.-Y. Liu, Y.-B. He, Influence of retrogression and reaging treatment on corrosion behaviour of an Al–Zn–Mg–Cu alloy, Mater. Des. 32 (4) (2011) 2149–2156.
[51] G.-s. Peng, K.-h. Chen, S.-y. Chen, H.-c. Fang, Influence of dual retrogression and reaging temper on microstructure, strength and exfoliation corrosion behavior of Al–Zn–Mg–Cu alloy, Trans. Nonferrous Metals Soc. China 22 (4) (2012) 803–809.